Weak Target Integration Detection Based on Radar Communication Integrated Signal via Constructed Step-LFM Model

Luhui XIAO [1,2], Xuan RAO [1], Wenbin HE [1], Hong YI [1], Jianfen HU [1]*

[1] Nanchang Hangkong University, Nanchang 330063, China
[2] Hubei Sanjiang Hangtian Xianfeng Electronic Information Co., Ltd, Xiaogan 432100, China

[*] ffeenn777@163.com

Submitted November 15, 2023 / Accepted February 21, 2024 / Online first March 11, 2024

Abstract. *Weak target detection is a great challenging in radar field. To detect weak targets via radar communication integrated signal, a method for constructed step-LFM (CStep-LFM) signal is proposed based on quadrature amplitude modulation-orthogonal frequency division multiplexing (QAM-OFDM) echoes. First, a QAM-OFDM and CStep-LFM model is established, and then a bandpass filters bank is used to transform the QAM-OFDM echo into a Step-LFM signal. Finally, compared with several existing integrated signals, the analyses and the simulation results show that CStep-LFM signal not only improves the detection performance of weak targets but also has a better communication performance.*

Keywords

Weak target detection, CStep-LFM, radar communication integrated signal, QAM-OFDM

1. Introduction

With the development of communication technology and radar technology, the problem of overlap between radar and communication in the frequency band is becoming more and more serious [1–3]. From the perspective of spectrum resources, the electromagnetic spectrum from 1 MHz to 100 GHz is a very precious spectrum resource. Some specific frequency bands, such as those below 5 GHz, have a long history of scarcity of spectrum resources, which has led to the competition between radar and telecommunication over spectrum resources. For the problem of spectrum competition and electromagnetic interference between radar and communication, the most promising solution at present is the integration of radar and communication (Joint Radar-Communication (RadCom)) [4–11], which utilizes the modulated signals transmitting in the same frequency band, efficiently utilizes all kinds of resources, and completes the two functions of information transmission and target detection in the same frequency at the same time.

Radar is widely used for target detection and tracking. It is worth noting that there are a large number of weak targets with low observability, and these weak targets have extremely low signal-to-noise ratios (SNR), which makes traditional radar detection algorithms unable to detect these weak targets effectively [12], [13]. To improve the detection performance of weak targets, an available way is long-time coherent integration. Increasing the integration time can effectively improve the SNR [14–16].

The radar communication integrated signal should not only achieve detection of weak targets and estimation of target motion parameters, but also transmission of communication information. Because the linear frequency modulation (LFM) [17], [18] signal has a large time bandwidth product and overcomes the contradiction between pulse energy and distance resolution by pulse compression, it has been used in the radar field for a long time. Integrated waveform design solutions for radar communication based on LFM signals have been widely explored. For example, by combining minimum frequency shift keying modulation (MSK) with LFM, the MSK-LFM [19–22] integrated signal has better ranging and velocity measurement performance. Similarly, QAM can be used instead of MSK to obtain QAM-LFM [23], [24] signals. However, the transmitted communication data is limited via MSK-LFM and QAM-LFM. So quadrature amplitude modulation-orthogonal frequency division multiplexing (QAM-OFDM) [25–29] is proposed to transmit more communication datum simultaneously, but has a low target detection performance. LFM-OFDM radar signal is mentioned in [30], which combines OFDM and LFM, but it does not carry communication data and the signal is more complex to implement.

The remainder of this paper is organized as follows. In Sec. 2, the QAM-OFDM signal model is established. CStep-LFM signal model is introduced in detail in Sec. 3. In Sec. 4, some numerical experiments are provided. Conclusions are given in Sec. 5.

DOI: 10.13164/re.2024.0195

2. QAM-OFDM Signal Model

Suppose that each pulse transmitted by a pulse Doppler radar is composed of N_s OFDM symbols. Then a single transmitted baseband pulse signal $s(t)$ could be expressed as

$$s(t)=\sum_{n=0}^{N_s-1}\sum_{m=0}^{N_c-1}\mathrm{rect}\left(\frac{t-nT_s}{T_s}\right)d_{n,m} \times\exp\left[\mathrm{j}2\pi\left(f_0+m\Delta f\right)\left(t-nT_s\right)\right] \tag{1}$$

where $d_{n,m}$ denotes the transmitted data, which is modulated by the m-th subcarrier of the n-th OFDM symbol, the number of OFDM symbols is N_s, the subcarrier number of OFDM symbols is N_c, f_0 is the initial subcarrier frequency, Δf is the subcarrier interval, the duration of OFDM symbols is T_s, $\mathrm{rect}\left(\frac{t}{T_s}\right)=\begin{cases}1, & |t|\le T_s/2\\ 0, & |t|>T_s/2\end{cases}$ is a rectangular window.

To ensure the subcarriers of the received signal can be completely separated during waveform construction, the subcarrier interval should satisfy the orthogonal condition, i.e.,

$$\Delta f=\frac{p}{T_p} \tag{2}$$

where $T_p=N_s\times T_s$ is the pulse width, p is a separation factor which is a positive integer and the minimal value of p is 1.

The two-dimensional echo signal of the QAM-OFDM integration signal can be expressed as:

$$s(\hat{t},t_m)=A_r\sum_{m=0}^{N_s-1}\sum_{n=0}^{N_c-1}\mathrm{rect}\left(\frac{\hat{t}-\frac{2r(t_m)}{c}-nT_s}{T_s}\right)d_{n,m}\exp\left(-\mathrm{j}\frac{4\pi f_c r(t_m)}{c}\right) \times\exp\left[\mathrm{j}2\pi\left(f_0+m\Delta f\right)\left(\hat{t}-\frac{2r(t_m)}{c}-nT_s\right)\right] \tag{3}$$

where $\hat{t}$ is the fast time, t_m is the slow time, A_r is the amplitude of the echo, c is the speed of light, f_c is the radar carrier frequency, $r(t_m)=R_0+vt_m$ is the distance between target and radar, R_0 is the initial distance, v is the radial velocity.

3. CStep-LFM Signal Model and Method

3.1 CStep-LFM Model

Both the stepped frequency signal and the LFM signal are broadband radar signals. CStep-LFM signal is a constructed step-LFM signal based on OFDM symbol and can be divided into several sub-pulses. The duration of each sub-pulse is T_p and the frequency of each sub-pulse remains unchanged but the frequency between adjacent sub-pulses keeps a step increasing, i.e., the step frequency is Δf. According to the spectrum, the constructed signal is similar to LFM. Thus, CStep-LFM signal can be given as follows:

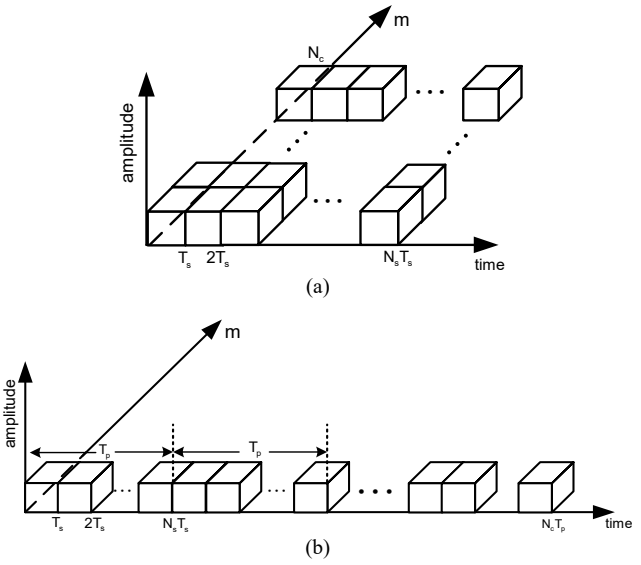

Fig. 1. CStep-LFM signal model. (a) OFDM signal. (b) CStep-LFM signal based on OFDM signal.

$$s_{\text{CStep-LFM}}(t)=\sum_{m=0}^{N_s-1}\sum_{n=0}^{N_s-1}\mathrm{rect}\left(\frac{t-nT_s}{T_s}\right)\mathrm{rect}\left(\frac{t-mT_p}{T_p}\right)d_{m,n} \times\exp\left[\mathrm{j}2\pi\left(f_0+m\Delta f\right)\left(t-nT_s\right)\right]. \tag{4}$$

CStep-LFM signal model is given in Fig. 1, where the m-axis represents the number of the subcarriers and the n-axis represents time, i.e., the number of the transmitted OFDM symbols, the variables N_s, N_c and T_s have the same meaning as in (1), T_p is the pulse width.

3.2 CStep-LFM Method

Let the QAM-OFDM echoes, transmitted by a pulse Doppler radar, pass through a bandpass filter bank and reconstruct the echoes based on the concept of parallel-to-serial conversion. According to the different subcarriers of the QAM-OFDM signal, the phase characteristic of each filter of the bandpass filters bank is adjusted to provide different output time delays, as shown in Fig. 2(a).

The frequency response characteristic of the bandpass filters bank is:

$$H_n(\mathrm{e}^{\mathrm{j}\omega})=H_n(\omega)\,\mathrm{e}^{-\mathrm{j}\omega(n-1)T_p} \tag{5}$$

where $H_n(\omega)$ is the magnitude characteristic which equals a constant, $-\mathrm{j}\omega(n-1)T_p$ is the phase characteristic and the range of n is $[1,N_c]$.

From (4), the phase characteristics of the filter of the bandpass filter bank vary with n. According to the time-shifting property, the time delay of the first subcarrier com-

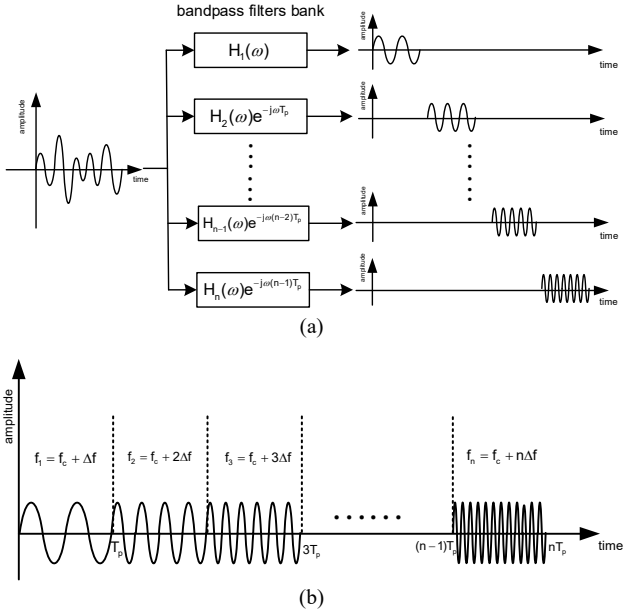

Fig. 2. Progress of constructing echo. (a) Separation of subcarrier via bandpass filters bank. (b) Reconstruction of echoes via parallel-to-serial conversion.

ponent is zero, the delay of the second is T_p, the third is 2 T_p, and so on. Then, reconstruct the echoes via parallel-to-serial conversion and the final constructed signal is shown in Fig. 2(b), in which it can be seen that the frequency of the echoes after reconstruction is increasing step by step and the duration of the constructed signal becomes $T_{cp} = N_c \times T_p$.

3.3 Radar Performance Analysis

3.3.1 Ambiguity Function

Ambiguity function is an important tool for radar waveform design and analysis. To show the radar performance of the CStep-LFM, the radar ambiguity function is analyzed in this section. The ambiguity function is defined in various ways and the following definition is adopted in this paper:

$$\chi(\tau, f_d) = \int_{-\infty}^{+\infty} s(t)s^*(t-\tau)\exp(j2\pi f_d t)\,dt \tag{6}$$

where τ is the time delay, f_d is the Doppler shift, $s^*(t)$ is the conjugate of $s(t)$.

After a delay τ, Equation (4) can be written as:

$$\begin{aligned} &s_{\text{CStep-LFM}}(t-\tau) = \\ &\sum_{m=0}^{N_c-1}\sum_{n=0}^{N_s-1}\text{rect}\left(\frac{t-\tau-nT_s}{T_s}\right)\text{rect}\left(\frac{t-\tau-mT_p}{T_p}\right)d_{m,n} \\ &\times\exp\left[j2\pi\left(f_0+m\Delta f\right)\left(t-\tau-nT_s\right)\right]. \end{aligned} \tag{7}$$

Substituting (4) and (7) into (6), then:

$$\begin{aligned} \chi(\tau, f_d) = &\int_{-\infty}^{+\infty}\sum_{m=0}^{N_c-1}\sum_{n=0}^{N_s-1}\text{rect}\left(\frac{t-nT_s}{T_s}\right)\text{rect}\left(\frac{t-mT_p}{T_p}\right)d_{m,n} \\ &\times\exp\left[j2\pi m\Delta f\left(t-nT_s\right)\right] \\ &\times\sum_{p=0}^{N_c-1}\sum_{q=0}^{N_s-1}\text{rect}\left(\frac{t-\tau-qT_s}{T_s}\right)\text{rect}\left(\frac{t-\tau-pT_p}{T_p}\right)d_{m,n}^* \\ &\times\exp\left[-j2\pi p\Delta f\left(t-\tau-qT_s\right)\right] \\ &\times\exp(j2\pi f_d t)\,dt \end{aligned} \tag{8}$$

where the variables N_s, N_c, $d_{m,n}$ and T_s have the same meaning as in (1), τ is the time delay, f_d is the Doppler shift, T_p is the pulse width.

To analyze conveniently, it is assumed that each subcarrier carries only a single communication data, and the ambiguity function can be simplified as:

$$\begin{aligned} \chi(\tau, f_d) = &\sum_{m=0}^{N_c-1}\text{rect}\left(\frac{t-mT_p}{T_p}\right)d_m\exp(j2\pi m\Delta f t) \\ &\times\sum_{p=0}^{N_c-1}\text{rect}\left(\frac{t-pT_p}{T_p}\right)d_p^*\exp\left[-j2\pi p\Delta f(t-\tau)\right] \\ &\times\exp(j2\pi f_d t). \end{aligned} \tag{9}$$

Equation (9) can be discussed by the cases given as follows:

(1) When $|\tau| \geq N_c T_p$, $\chi(\tau, f_d) = 0$, where $|\tau|$ represents the absolute value of τ.

(2) When $-N_c T_p < \tau < 0$ and $\lfloor \tau/T_p \rfloor = k$, $\lfloor x \rfloor$ means that x is rounded down. The calculation of ambiguity function for time delay less than 0 is shown in Fig. 3. In Fig. 3, ambiguity function according to the integral range, the expression contains two integral terms. Define $\tau' = \tau + (1+|k|)T_p$, $\tau'' = \tau + |k|T_p$, then $\tau' = \tau'' + T_p$, $-T_p < \tau'' \leq 0$, $0 < \tau' \leq T_p$, the ambiguity function can be expressed as:

$$\begin{aligned} \chi(\tau, f_d) = &\sum_{m=0}^{N_c-1-|k|}\exp\left\{j2\pi m f_d T_s\right\}\chi^-_{m,m+|k|}(\tau'', f_d) \\ &+\sum_{m=1}^{N_c-1-|k|}\exp\left\{j2\pi(m-1)f_d T_s\right\}\chi^+_{m-1,m+|k|}(\tau', f_d). \end{aligned} \tag{10}$$

(3) When $-N_c T_p < \tau < 0$ and $\lfloor \tau/T_p \rfloor = k$ the calculation of ambiguity function for time delay greater than 0 is shown in Fig. 4. Define $\tau' = \tau - kT_p$, $\tau'' = \tau - (|k|+1)T_p$, then $\tau' = \tau'' + T_p$, $0 < \tau' \leq T_p$, $-T_p < \tau'' \leq 0$, the ambiguity function can be expressed as:

$$\begin{aligned} \chi(\tau, f_d) = &\sum_{p=0}^{N_c-1-|k|}\exp\left\{j2\pi(|k|+p)f_d T_s\right\}\chi^+_{|k|+p,p}(\tau', f_d) \\ &+\sum_{p=1}^{N_c-1-|k|}\exp\left\{j2\pi(|k|+p)f_d T_s\right\}\chi^-_{|k|+p,p-1}(\tau'', f_d). \end{aligned} \tag{11}$$

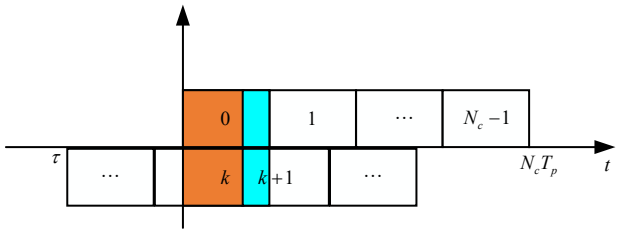

Fig. 3. Diagram of the calculation of ambiguity function for time delay less than 0.

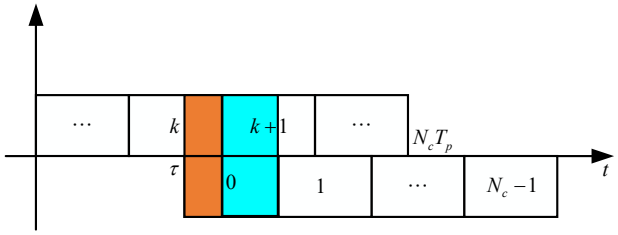

Fig. 4. Diagram of the calculation of ambiguity function for time delay greater than 0.

The $\chi^{-}_{m,p}(\tau,f_d)$, $\chi^{+}_{m,p}(\tau,f_d)$ in (10) and (11) denote the mutual ambiguity function between the m-th subcarrier and the p-th subcarrier when τ satisfies $-T_p \le \tau \le 0$ and $0 < \tau < T_p$, respectively.

(1) When $-T_p \le \tau \le 0$, the integration of the mutual ambiguity function is (Fig. 5):

$$\begin{aligned}\chi^{-}_{m,p}(\tau,f_d) &= (T_p+\tau)d_m d_p^* \exp(\mathrm{j}2\pi p\Delta f\tau)\\ &\times\exp\left\{\mathrm{j}\pi[(m-p)\Delta f+f_d](T_p+\tau)\right\}\\ &\times\mathrm{sinc}\left\{\pi[(m-p)\Delta f+f_d](T_p+\tau)\right\}.\end{aligned} \tag{12}$$

(2) When $0 < \tau < T_p$, the integration of the mutual ambiguity function is (Fig. 6):

$$\begin{aligned}\chi^{+}_{m,p}(\tau,f_d) &= (T_p-\tau)d_m d_p^* \exp(\mathrm{j}2\pi p\Delta f\tau)\\ &\times\exp\left\{\mathrm{j}\pi[(m-p)\Delta f+f_d](T_p-\tau)\right\}\\ &\times\mathrm{sinc}\left\{\pi[(m-p)\Delta f+f_d](T_p-\tau)\right\}.\end{aligned} \tag{13}$$

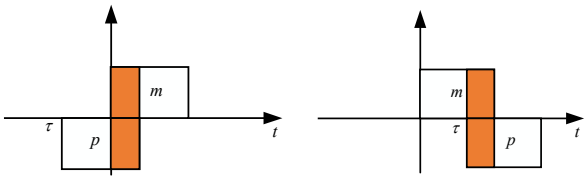

Fig. 5. Diagram of the calculation of mutual ambiguity function. (a) Case for time delay less than 0. (b) Case for time delay greater than 0.

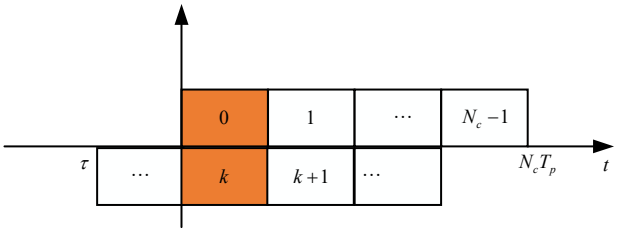

Fig. 6. Case for time delay is an integer multiple of T_p.

Substituting (12) and (13) into (10) and (11), then the ambiguity function is:

(1) When $-N_cT_p < \tau < 0$

$$\begin{aligned}\chi(\tau,f_d) &= (T_p+\tau)\sum_{m=0}^{N_c-1-|k|}\exp\left\{\mathrm{j}2\pi m f_d T_s\right\}d_m d_{m+|k|}^*\\ &\times\exp(\mathrm{j}2\pi(m+|k|)\Delta f\tau'')\\ &\times\exp\left\{\mathrm{j}\pi[f_d-|k|\Delta f](T_p+\tau'')\right\}\\ &\times\mathrm{sinc}\left\{\pi[f_d-|k|\Delta f](T_p+\tau'')\right\}\\ &+(T_p-\tau)\sum_{m=1}^{N_c-1-|k|}\exp\left\{\mathrm{j}2\pi(m-1)f_d T_s\right\}d_{m-1}d_{m+|k|}^*\\ &\times\exp(\mathrm{j}2\pi(m+|k|)\Delta f\tau')\\ &\times\exp\left\{\mathrm{j}\pi[(-1-|k|)\Delta f+f_d](T_p-\tau')\right\}\\ &\times\mathrm{sinc}\left\{\pi[(-1-|k|)\Delta f+f_d](T_p-\tau')\right\}.\end{aligned} \tag{14}$$

(2) When $0 < \tau < N_cT_p$

$$\begin{aligned}\chi(\tau,f_d) &= \sum_{p=0}^{N_c-1-|k|}\exp\left\{\mathrm{j}2\pi(|k|+p)f_d T_s\right\}(T_p-\tau')d_{|k|+p}d_p^*\\ &\times\exp(\mathrm{j}2\pi p\Delta f\tau')\\ &\times\exp\left\{\mathrm{j}\pi[|k|\Delta f+f_d](T_p-\tau')\right\}\\ &\times\mathrm{sinc}\left\{\pi[|k|\Delta f+f_d](T_p-\tau')\right\}\\ &+\sum_{p=1}^{N_c-1-|k|}\exp\left\{\mathrm{j}2\pi(|k|+p)f_d T_s\right\}(T_p+\tau'')d_{|k|+p}d_{p-1}^*\\ &\times\exp(\mathrm{j}2\pi(p-1)\Delta f\tau'')\\ &\times\exp\left\{\mathrm{j}\pi[(|k|+1)\Delta f+f_d](T_p+\tau'')\right\}\\ &\times\mathrm{sinc}\left\{\pi[(|k|+1)\Delta f+f_d](T_p+\tau'')\right\}.\end{aligned} \tag{15}$$

From (14) and (15), the ambiguity function $\chi(\tau,f_d)$ of the integrated signal is not only affected by the time delay τ and Doppler shift f_d, but also by the communication information, as well as the subcarrier interval Δf.

A discussion of the above special case is given when τ is exactly an integer multiple of T_p (Fig. 6), that is, $-N_cT_p < \tau = kT_p < 0$. The ambiguity function can be expressed as:

$$\begin{aligned}\chi(\tau,f_d) &= T_p\sum_{m=0}^{N_c-1-|k|}d_m d_{m+|k|}^*\exp\left[\mathrm{j}2\pi(m+|k|)\Delta f\tau\right]\\ &\times\exp\left[\mathrm{j}\pi(f_d-|k|\Delta f)T_p\right]\\ &\times\mathrm{sinc}\left[\mathrm{j}\pi(f_d-|k|\Delta f)T_p\right].\end{aligned} \tag{16}$$

The zero delay transversal and zero Doppler transversal are given as follows, respectively:

$$\begin{aligned}\chi(0,f_d) &= T_p\sum_{m=0}^{N_c-1-|k|}d_m d_{m+|k|}^*\exp\left[\mathrm{j}\pi(f_d-|k|\Delta f)T_p\right]\\ &\times\mathrm{sinc}\left[\mathrm{j}\pi(f_d-|k|\Delta f)T_p\right],\end{aligned} \tag{17}$$

$$\chi(\tau,0)=T_p\sum_{m=0}^{N_c-1-|k|}d_m d_{m+|k|}^{*}\exp\left[\mathrm{j}2\pi(m+|k|)\Delta f\tau\right]\times\exp\left[-\mathrm{j}\pi|k|\Delta fT_p\right]\mathrm{sinc}\left[-\mathrm{j}\pi|k|\Delta fT_p\right]. \quad (18)$$

As can be seen from (17) and (18), when the subcarrier interval Δf is very small, its ambiguity function will be approximated towards the LFM ambiguity function. Similarly, this phenomenon happens in the case of $0<\tau=kT_p<N_cT_p$.

3.3.2 Pulse Compression Gain

To detect target in low SNR, the gain of CStep-LFM signal is analyzed. Define the total gain as G_{total}, then

$$G_{\text{total}}=G_{\text{PC}}+G_{\text{MTD}} \quad (19)$$

where G_{PC} is the pulse compression gain, and G_{MTD} is the coherent integration gain of the moving target detection (MTD) algorithm.

The total gain G_{total} is the sum of both the pulse compression gain G_{PC} and the coherent integration gain G_{MTD}. The G_{MTD} is fixed when the pulse number of integration is given for a target with a constant radial velocity, the only improved factor is the G_{PC} after the echoes are reconstructed according to the method proposed in this paper. The G_{PC} will increase with the increasing of the time width of the signal, which is given as follows

$$G_{\text{PC}}=10\log_{10}(N_c\times T_p\times B) \quad (20)$$

where B is the signal bandwidth.

3.4 Communication Performance Analysis

3.4.1 Bit Error Rate (BER)

Communication performance can be measured by BER. The demodulation process of OFDM integrated waveform is shown in Fig. 7.

After down-conversion, the subcarriers are separated by DFT, and then the data on each subcarrier is mapped by constellation. The modulation method used in this paper is 16QAM, then the theoretical BER of the QAM-OFDM signal can be expressed as:

$$P_e=1-\left(1-\frac{3}{4}\mathrm{erfc}\sqrt{\frac{1}{20}SNR}\right)^2. \quad (21)$$

3.4.2 Communications Rate

In this paper, OFDM technology is adopted, which has multiple subcarriers, and the communication rate is N_c times higher than that of single-carrier system integrated signal. The communication rate can be represented as:

$$R_b=\frac{N_c\log_2 M}{T_s} \quad (22)$$

where M is the modulated number.

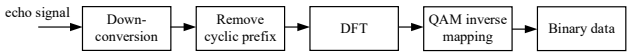

Fig. 7. OFDM demodulation process.

According to (22), the communication rate is related to the modulated number M, the number N_c of subcarriers and the symbol period T_s of the integrated signal. When the communication rate of OFDM is improved, the BER will be decreased at the same time. To make the integrated signal communication performance better, the communication rate and BER should keep a good level as far as possible during the parameter design.

4. Simulation Results

4.1 Radar Performance

4.1.1 Ambiguity Function

The ambiguity function of QAM-OFDM and CStep-LFM are obtained through simulation. The OFDM simulation parameters are set as follows: the pulse width is $T_p=10$ μs, and the signal bandwidth is $B=10$ MHz, the OFDM symbols $N_s=20$.

Figure 8 shows the ambiguity function, zero Doppler section and zero delay section of OFDM and CStep-LFM respectively. It can be seen in Fig. 8(a) and Fig. 8(b) that the ambiguity functions of OFDM and CStep-LFM signals are similar to thumbtack shape and have sidelobes for the influence of communication data. From zero Doppler section and zero delay section, the sidelobe of OFDM is higher than that of CStep-LFM, which indicates that CStep-LFM has a better Doppler resolution and delay resolution.

4.1.2 Weak Target Detection

In the simulation, the proposed method is compared with QAM-OFDM, QAM-LFM, LFM-OFDM and MSK-LFM, where the data modulation of both QAM-LFM, LFM-OFDM and QAM-OFDM is 16QAM. In this paper, Monte Carlo method is used for simulation to analyze the weak target detection performance. The experiment parameters are given as follows: $R_0=200$ km, $v=10$ m/s, $B=40$ MHz, $T_p=2$ μs, $PRF=3000$, the integration time is $T_{\text{integration}}=0.1$ s, the subcarrier number N_c of OFDM is set to 10, the OFDM symbols $N_s=5$, the probability of false alarm is $P_{fa}=10^{-6}$, the number of Monte Carlo experiments is 3000 times.

When the input SNR varies from –50 to –20 dB, the relationship curve between detection probability P_d and the input SNR is shown in Fig. 9. From Fig. 9, when $SNR=-30$ dB, the P_d of MSK-LFM and QAM-LFM reaches 1, and when $SNR=-35$ dB and $SNR=-40$ dB, the P_d of QAM-OFDM and CStep-LFM,OFDM-LFM reaches 1 respectively. It is clear that the CStep-LFM can improve the weak target detection performance. According to (20), the improved gain can be calculated as $10\log_{10}N_c=10$ dB,

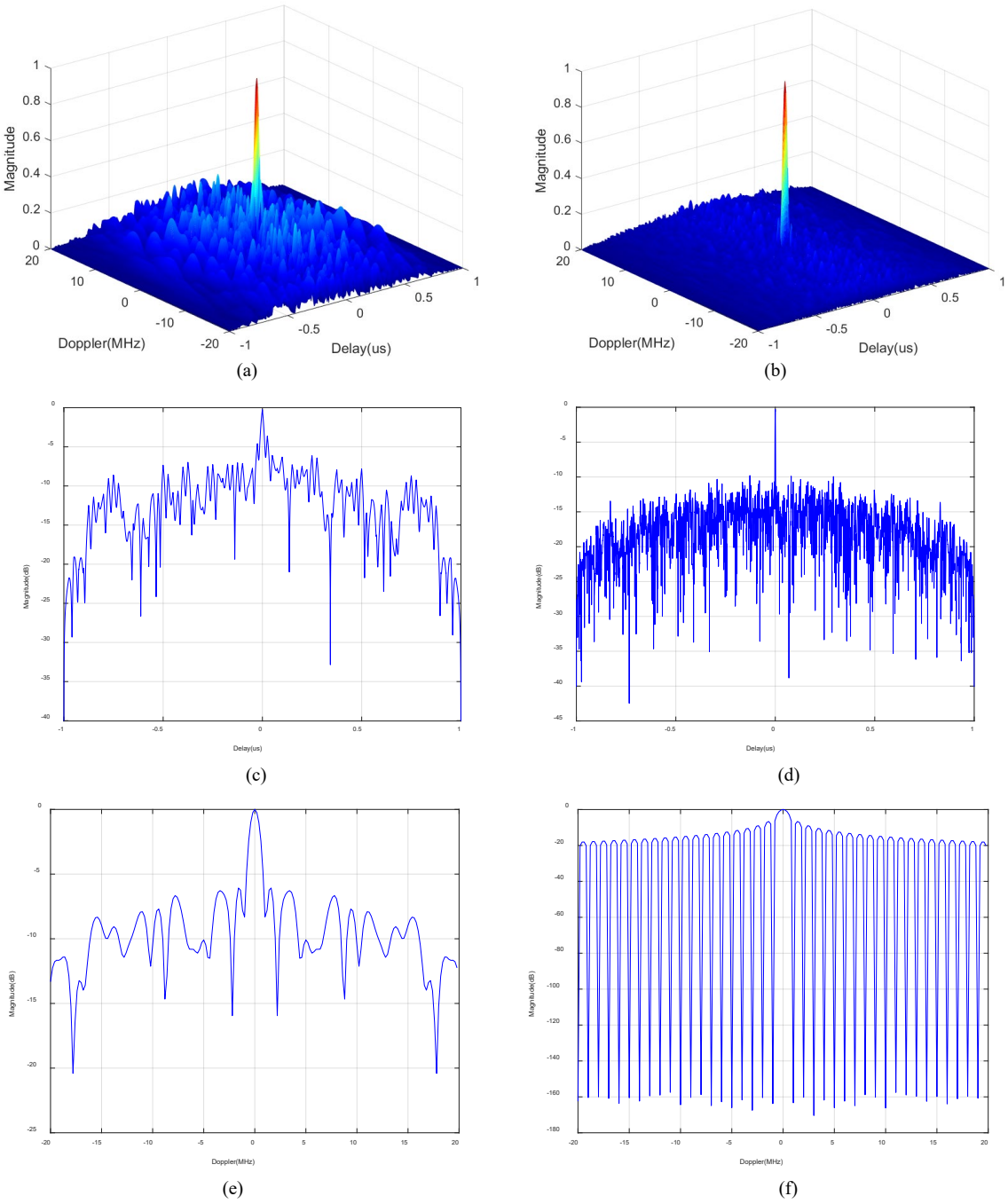

Fig. 8. Ambiguity function simulation. (a) OFDM ambiguity function. (b) CStep-LFM ambiguity function. (c) OFDM zero Doppler section. (d) CStep-LFM zero Doppler section. (e) OFDM zero delay section. (f) CStep-LFM zero delay section.

which is consistent with the result of the simulation experiment. The P_d of CStep-LFM and OFDM-LFM reaches 1 at the same SNR, but CStep-LFM is easier to implement in practice.

4.2 Communication Performance

Assume the channel is Gaussian white noise channel, the SNR varies from 0 to 25 dB, and the subcarrier number N_c of OFDM is set to 10. For MSK-LFM and 16QAM-LFM, which are single carriers, OFDM can transmit more data as described in Sec. 3.4.2. In the simulation, MSK-LFM and 16QAM-LFM transmit 10 bits of data per pulse and then the pulse repetition frequency is $PRF = 3000$, so the capacity of data that can be transferred per second is 30 kbit. According to (22), it can be seen that the transmission rate is related to N_c. When $N_c = 10$, the 16QAM-OFDM and MFM-OFDM can transmit 300 kbits of data per second. In general, OFDM can achieve high-speed, high-capacity transmission of data. The BER of MSK-LFM, 16QAM-LFM, LFM-OFDM and 16QAM-OFDM is shown in Fig. 10 and the communication rate is shown in Tab. 1.

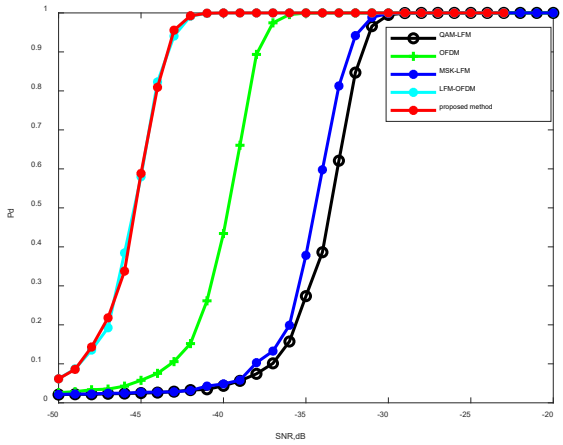

Fig. 9. Detection probability P_d of QAM-OFDM (CStep-LFM), QAM-OFDM, MSK-LFM, OFDM-LFM and QAM-LFM.

Radar communication integrated signal	Communication rate (kbit/s)
16QAM-OFDM	300
LFM-OFDM	300
MSK-LFM	30
16QAM-LFM	30

Tab. 1. Communication rate of 16QAM-OFDM, 16QAM-LFM, LFM-OFDM and MSK-LFM.

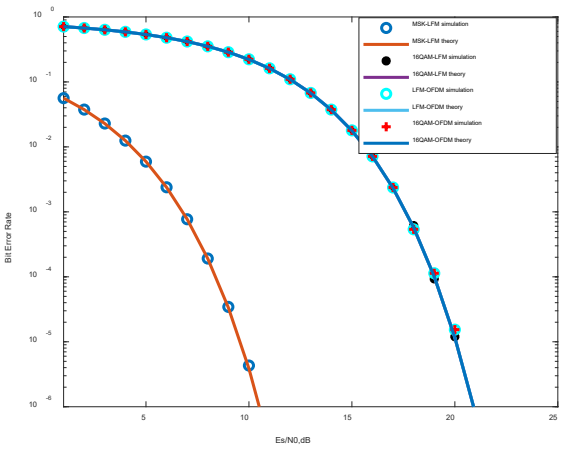

Fig. 10. BER of 16QAM-OFDM, MSK-LFM LFM-OFDM and 16QAM-LFM.

From Fig. 10, it can be seen that the theoretical BER of 16QAM-OFDM and the BER of the simulation experiment basically coincide, and the BER of MSK-LFM is better, but its communication rate is low. In Tab. 1, compared with MSK-LFM, QAM-LFM, 16QAM-OFDM and LFM-OFDM has better communication rates, but its BER decreases. The reason is that a certain amount of BER performance is sacrificed in higher-order modulation to improve signal bandwidth utilization and the bit rate of the signal transmission. In the case of the same SNR, the higher the order of QAM is, the worse the BER performance is. But the higher the order of QAM is, the higher the spectrum will be utilized.

5. Conclusion

The CStep-LFM method is proposed to enhance the detection performance of radar communication integrated signal on weak targets detection. Based on the idea of series-parallel conversion, the QAM-OFDM pulse signals are transmitted, and the echoes are reconstructed as a step-LFM signal to increase the time width of the echoes, which will increase the pulse compression gain and enhance the weak target detection performance. According to the simulation results, the CStep-LFM method is effective. Compared to LFM-OFDM, CStep-LFM can achieve the same effect. The difference between LFM-OFDM and Cstep-LFM is that one of the subcarriers is LFM and the other is a single-carrier signal, and these subcarriers need to be orthogonal to each other. In practical implementation, the difficulty of generating orthogonal single-carrier will be lower than that of LFM.

Acknowledgments

The authors would like to thank the anonymous reviewers and the Associate Editor. This work is supported by the National Nature Science Foundation of China under Grant 62161029, the Jiangxi Provincial Natural Science Foundation under Grants 20202BABL202002, SAST2018078, the Doctoral Scientific Research Foundation of NCHU under Grant EA201804195.

References

[1] ZHANG, Z., NAJAFABADI, H. E., LEUNG, H. Array resource allocation for radar and communication integration network. *Signal Processing*, 2020, vol. 176, p. 1–9. DOI: 10.1016/j.sigpro.2020.107701

[2] ZHANG, Z., NAJAFABADI, H. E., JIN, B. Transmit array resource allocation for radar and communication integration system. *Measurement*, 2020, vol. 173, no. 8, p. 1–9. DOI: 10.1016/j.measurement.2020.108595

[3] KIM, S. Radio resource management scheme in radar and communication spectral coexistence platform. *Computer Networks*, 2023, vol. 230, p. 1–9. DOI: 10.1016/j.comnet.2023.109773

[4] FENG, Z., FANG, Z., WEI, Z., et al. Joint radar and communication: A survey. *China Communications*, 2020, vol. 17, no. 1, p. 1–27. DOI: 10.23919/JCC.2020.01.001

[5] HONG, H., ZHAO, J., HONG, T., et al. Radar–communication integration for 6G massive IoT services. *IEEE Internet of Things Journal*, 2022, vol. 9, no. 16, p. 14511–14520. DOI: 10.1109/JIOT.2021.3064072

[6] ZHANG, J. A., LIU, F., MASOUROS, C., et al. An overview of signal processing techniques for joint communication and radar sensing. *IEEE Journal of Selected Topics in Signal Processing*,

2021, vol. 15, no. 6, p. 1295–1315. DOI: 10.1109/JSTSP.2021.3113120

[7] LIU, F., ZHENG, L., CUI, Y., et al. Seventy years of radar and communications: The road from separation to integration. *IEEE Signal Processing Magazine*, 2023, vol. 40, no. 5, p. 106–121. DOI: 10.1109/MSP.2023.3272881

[8] XU, R., PENG, L., ZHAO, W., et al. Radar mutual information and communication channel capacity of integrated radar-communication system using MIMO. *ICT Express*, 2015, vol. 1, no. 3, p. 102–105. DOI: 10.1016/j.icte.2016.01.001

[9] GAMEIRO, A., CASTANHEIRA, D., SANSON, J., et al. Research challenges, trends and applications for future joint radar communications systems. *Wireless Personal Communications*, 2018, vol. 100, no. 1, p. 81–96. DOI: 10.1007/s11277-018-5614-8

[10] GU, Y., ZHANG, L., ZHOU, Y., et al. Waveform design for integrated radar and communication system with orthogonal frequency modulation. *Digital Signal Processing*, 2018, vol. 83, p. 129–138. DOI: 10.1016/j.dsp.2018.08.014

[11] JIANG, M., LIAO, G., YANG, Z., et al. Integrated radar and communication waveform design based on a shared array. *Signal Processing*, 2020, vol. 182, no. 1, p. 1–11. DOI: 10.1016/j.sigpro.2020.107956

[12] LI, X., SUN, Z., YEO, T. S., et al. STGRFT for detection of maneuvering weak target with multiple motion models. *IEEE Transactions on Signal Processing*, 2019, vol. 67, no. 7, p. 1902 to 1917. DOI: 10.1109/TSP.2019.2899318

[13] RAO, X., TAO, H., SU, J., et al. Axis rotation MTD algorithm for weak target detection. *Digital Signal Processing*, 2014, vol. 26, p. 81–86. DOI: 10.1016/j.dsp.2013.12.003

[14] HUANG, P., XIA, X. G., LIAO, G., et al. Long-time coherent integration algorithm for radar maneuvering weak target with acceleration rate. *IEEE Transactions on Geoscience and Remote Sensing*, 2019, vol. 57, no. 6, p. 3528–3542. DOI: 10.1109/TGRS.2018.2885508

[15] ZUO, L., WANG, J., WANG, J., et al. UAV detection via long-time coherent integration for passive bistatic radar. *Digital Signal Processing*, 2021, vol. 112, p. 1–13. DOI: 10.1016/j.dsp.2021.102997

[16] CHEN, X., GUAN, J., CHEN, W., et al. Sparse long-time coherent integration-based detection method for radar low-observable manoeuvring target. *IET Radar, Sonar & Navigation*, 2020, vol. 14, no. 4, p. 538–546. DOI: 10.1049/iet-rsn.2019.0313

[17] LIU, X., XIAO, B., WANG, C. Optimal target function for the fractional Fourier transform of LFM signals. *Circuits, Systems, and Signal Processing*, 2022, vol. 41, no. 7, p. 4160–4173. DOI: 10.1007/s00034-022-01977-w

[18] KIM, D. H., KIM, H. J., LIM, J. H. Design of optimized coded LFM waveform for spectrum shared radar system. *Sensors*, 2021, vol. 21, no. 17, p. 1–13. DOI: 10.3390/s21175796

[19] CHEN, X., LIU, Z., LIU, Y., et al. Energy leakage analysis of the radar and communication integrated waveform. *IET Signal Processing*, 2018, vol. 12, no. 3, p. 375–382. DOI: 10.1049/iet-spr.2017.0248

[20] DOU, Z., ZHONG, X., ZHANG, W. Radar-communication integration based on MSK-LFM spread spectrum signal. *International Journal of Communications, Network and System Sciences*, 2017, vol. 10, no. 8B, p. 108–117. DOI: 10.4236/ijcns.2017.108B012

[21] MA, H., WANG, J., SUN, X., et al. Joint radar-communication relying on NLFM-MSK design. *Wireless Communications and Mobile Computing*, 2022, vol. 2022, p. 1–26. DOI: 10.1155/2022/4711132

[22] ZHANG, W., ZHANG, H. The design of integrated waveform based on MSK-LFM signal. In *15th IEEE International Conference on Signal Processing (ICSP)*. Beijing (China), 2020, p. 565–569. DOI: 10.1109/ICSP48669.2020.9320941

[23] MA, Q., LU, J., MAOXIANG, Y. Integrated waveform design for 64QAM-LFM radar communication. In *IEEE 5th Advanced Information Technology, Electronic and Automation Control Conference (IAEAC)*. Chongqing (China), 2021, p. 1615–1625. DOI: 10.1109/IAEAC50856.2021.9390784

[24] ZHAO, J., LI, J., YI, Y. Research on radar communication integrated signal based on 64QAM-LFM. In *International Wireless Communications and Mobile Computing (IWCMC)*. Harbin City (China), 2021, p. 1151–1155. DOI: 10.1109/IWCMC51323.2021.9498961

[25] LIU, Y., LIAO, G., XU, J., et al. Adaptive OFDM integrated radar and communications waveform design based on information theory. *IEEE Communications Letters*, 2017, vol. 21, no. 10, p. 2174–2177. DOI: 10.1109/LCOMM.2017.2723890

[26] LIU, Y., LIAO, G., YANG, Z., et al. Multiobjective optimal waveform design for OFDM integrated radar and communication systems. *Signal Processing*, 2017, vol. 141, p. 331–342. DOI: 10.1016/j.sigpro.2017.06.026

[27] RONG, J., LIU, F., MIAO, Y. Integrated radar and communications waveform design based on multi-symbol OFDM. *Remote Sensing*, 2022, vol. 14, no. 19, p. 1–22. DOI: 10.3390/rs14194705

[28] HUANG, Y., HU, S., MA, S., et al. Designing low-PAPR waveform for OFDM-based RadCom systems. *IEEE Transactions on Wireless Communications*, 2022, vol. 21, no. 9, p. 6979–6993. DOI: 10.1109/TWC.2022.3153606

[29] YE, M. K., ZHU, Q., DAI, P. C., et al. Design of QAM-OFDM radar-communication integrated signal based on Golay complementary sequences. *Journal of Physics: Conference Series*, 2021, vol. 2085, no. 1, p. 1–10. DOI: 10.1088/1742-6596/2085/1/012010

[30] LIU, Z., QUAN, Y., WU, Y., et al. Range and Doppler reconstruction for sparse frequency agile linear frequency modulation-orthogonal frequency division multiplexing radar. *IET Radar, Sonar & Navigation*, 2022, vol. 16, no. 6, p. 1014–1025. DOI: 10.1049/rsn2.12239

About the Authors …

Luhui XIAO was born in Jiangxi Province, China, in 1999. He received the B.Eng. degree in Electronic Information Engineering from the Nanchang Hangkong University, China, in 2021. He is currently pursuing the M.S. degree in Signal Processing from the School of Information Engineering, Nanchang Hangkong University. His current research interests include radar signal processing, radar communication integration and weak target detection.

Xuan RAO was born in Jiangxi Province, P.R. China, in 1977. He received the B.Sc. and M.Sc. degrees from the School of Information Engineering, Nanchang University, Nanchang, China, in 1999 and 2005, respectively; and the Ph.D. degrees from the School of Electronic Engineering, Xidian University, Xi'an, China, in 2015. He is currently an Associate Professor of the School of Information Engineering, Nanchang Hangkong University, China. He is

a member of IEEE and his current research interests include radar signal processing, weak target detection and tracking.

Wenbin HE was born in Hebei Province, China, in 1999. She received the B.Eng. degree in Electronic Information Engineering from the University of Jinan, China, in 2021. She is currently pursuing the M.S. degree in Signal Processing from the School of Information Engineering, Nanchang Hangkong University. Her current research interests include radar signal processing and weak target detection.

Hong YI was born in Jiangxi Province, P.R. China, in 1977. She received the Master degree in Computer Science from the School of Measuring and Control Engineering, Nanchang Hangkong University, Nanchang, China, in 2006. She is currently a lecturer of the School of Information Engineering, Nanchang Hangkong University, China. Her current research interests include control theory and control engineering.

Jianfen HU (corresponding author) was born in Jiangxi Province, P.R. China, in 1978. She received the Master degree from the School of Measuring and Control Engineering, the Northwestern Polytechnical University, Xi'an, China, in 2005. Her current research interests include signal processing, weak target detection and tracking.